Cerebral Cortex October 2015;25:3314–3329
doi:10.1093/cercor/bhu128
Advance Access publication June 26, 2014

Identification of Eye-Specific Domains and Their Relation to Callosal Connections in Primary Visual Cortex of Long Evans Rats

R.J. Laing[1,2], J. Turecek[1], T. Takahata[3] and J.F. Olavarria[1,2]

[1]Department of Psychology, and [2]Behavior and Neuroscience Program, University of Washington, Seattle, WA 98195-1525, USA and [3]Department of Psychology, Vanderbilt University, Nashville, TN 37240, USA

Address correspondence to Jaime Olavarria, Department of Psychology, University of Washington, Box 351525, Seattle, WA 98195-1525, USA. Email: jaime@uw.edu

Ocular dominance columns (ODCs) exist in many primates and carnivores, but it is believed that they do not exist in rodents. Using a combination of transneuronal tracing, in situ hybridization for Zif268 and electrophysiological recordings, we show that inputs from both eyes are largely segregated in the binocular region of V1 in Long Evans rats. We also show that, interposed between this binocular region and the lateral border of V1, there lies a strip of cortex that is strongly dominated by the contralateral eye. Finally, we show that callosal connections colocalize primarily with ipsilateral eye domains in the binocular region and with contralateral eye input in the lateral cortical strip, mirroring the relationship between patchy callosal connections and specific sets of ODCs described previously in the cat. Our results suggest that development of cortical modular architecture is more conserved among rodents, carnivores, and primates than previously thought.

Keywords: binocular, columnar organization, interhemispheric connections, ocular dominance columns, striate cortex

Introduction

In primary visual cortex (V1, area 17), ocular dominance columns (ODCs, aggregates of cells with the same eye preference), and orientation columns (aggregates of cells selective for the same orientation of edges or bar-like stimuli) have been extensively studied in a variety of mammalian species (Tootell et al. 1988; reviewed in Horton and Hocking 1996; Van Hooser 2007). These studies revealed that while ocular dominance and orientation columns are evident in many carnivores and primates, there is little evidence of their existence in V1 of other orders such as rodents (Dräger 1975; Metín et al. 1988; Fagiolini et al. 1994; Gordon and Stryker 1996; Antonini et al. 1999; Girman et al. 1999; Ohki et al. 2005; Ohki and Reid 2007). This apparent difference between animal groups suggests that mammals can be broadly divided into species that have columnar architecture in visual cortex and those that do not (Horton and Hocking 1996; Van Hooser 2007). Surprisingly, response tuning properties of visual cortical neurons do not seem to depend on the existence of orientation columns because these properties are remarkably similar in animals with and without orientation columns (Girman et al. 1999; Van Hooser et al. 2005, 2006). These observations have cast doubt on the idea that wiring of functional visual cortical circuits follows the same master plan in all species (Horton and Adams 2005; Van Hooser 2007). In addition, the lack of ocular dominance and orientation columns in the gray squirrel—a diurnal, highly visual rodent whose brain size compares to that of animals with ocular dominance and orientation columns—implies that the absence of columnar architecture in visual cortex in rodents cannot be attributed solely to their small brain or nocturnal habit (Van Hooser et al. 2005, 2006). Instead, these studies have led to the idea that in animals like rodents, functional architecture in visual cortex is fundamentally different from that in carnivores and primates.

In the cat, visual callosal connections form patches that are closely correlated with ODCs (Olavarria 2001, 2002). Prompted by preliminary observations that callosal connections are also patchy in Rat V1 we set out to investigate whether callosal patches reflect an underlying pattern of ocular dominance domains that has not been previously described in the rat. We examined this possibility using a combination of anatomical and functional approaches. We found that inputs from both eyes segregate into eye-specific domains in a binocular region of V1. Moreover, we found that in this region callosal patches correlate primarily with ipsilateral eye domains. Surprisingly, our results also show that between this binocular region and the lateral border of V1 lies a narrow, callosal rich region that is dominated nearly exclusively by the contralateral eye.

Materials and Methods

Normal adult Long Evans hooded rats (*Rattus norvegicus*, Charles River Laboratories) were used and procedures were performed according to protocols approved by the Institutional Animal Care and Use Committee at the University of Washington and Vanderbilt University, and are in accordance with the animal care guidelines of the National Institutes of Health, USA.

Intraocular and Intracortical Injections of Anatomical Tracers and Histochemical Processing

Intraocular and intracortical tracer injections were performed under anesthesia induced and maintained with isoflurane (5 and 2.5%, respectively) in air. Retino-thalamo-cortical projections were revealed following intravitreal injections of the transneuronal tracer horseradish peroxidase conjugated to wheat-germ agglutinin (WGA-HRP; Sigma Co.). Due to its transneuronal transport property, demonstrated at the ultrastructural level (Itaya and Van Hoesen 1982), this tracer has been widely used in studies of retino-thalamo-cortical projections in a variety of species, including rats (Gerfen et al. 1982; Itaya and Van Hoesen 1982; Kageyama et al. 1990), cats (Anderson et al. 1988; Olavarria 2001), ferret (Ruthazer et al. 1999; White et al. 1999), and monkeys (Horton and Hocking 1996). Moreover, cortical patterns of WGA-HRP labeling interdigitate with patterns labeled from the opposite eye with tritiated proline—another widely used transneuronal tracer—in cats (Hata and Stryker 1994) and monkeys (Horton and Hocking 1996), providing evidence that WGA-HRP patterns represent ODCs. A total volume of 6 μL of 3% WGA-HRP in saline was pressure injected over ~15 min through glass micropipettes (50–100 μm tip diameter). The injection site was ~2.0 mm posterior to the corneal limbus, at a depth of ~2.0 mm. Callosal connections were labeled following multiple intracortical injections of either horseradish peroxidase

(HRP, Sigma Co, 25% in saline; total volume = 4.0 μL), biotinylated biodextran amine (BDA, 10 kDa, 10% in 0.9% saline, Molecular Probes, Eugene, Oregon, total volume = 4 μL), or rhodamine-tagged latex beads (RB; LumaFlour, Naples, FL, concentrated stock solution, total volume = 4 μL). Previous studies at both light and electron microscopic levels have demonstrated that HRP is transported both anterogradely and retrogradely (Trojanowski et al. 1981), while BDA (10 kDa) is transported mainly anterogradely, although some retrograde labeling may occur (Reiner et al. 2000). The fluorescent tracer RB is transported retrogradely (Katz et al. 1984).

For all intracortical tracers used, evenly spaced injections (0.2 μL each) were delivered at a depth of ~800–1000 μm in occipital cortex. The tracers were pressure injected through glass micropipettes (50–100 μm tip diameter) over an area extending ~2–7 mm lateral to midline suture, and 0.0–6.0 mm anterior to lambda suture. During the tracer injections, the dura was kept intact and moist with saline. Following the injections, the bone chip was repositioned and the skin was sutured by planes.

Four days following intraocular injections of WGA-HRP and 2–3 days following intracortical injections of anatomical tracers (HRP, BDA, or RB) animals were deeply anesthetized with pentobarbital sodium (100 mg/kg i.p.) and perfused through the heart with 0.9% saline followed by 4% paraformaldehyde (PFA) in 0.1 M phosphate buffer (PB) (pH 7.4). Cortical mantles were either separated from the brains and flattened for sectioning in the tangential plane or left intact for sectioning in the coronal plane. The flattened cortices were left between glass slides for 24 h in 0.1 M PB, after which time the tissue was transferred to a 4% PFA in 0.1 M PB, 20% sucrose solution for ~1 additional hour. Tissue blocks to be sectioned in the coronal plane were kept in 4% PFA in 0.1 M PB and 20% sucrose for one or more days. All tissue was cut on a freezing microtome at 60 μm thickness and the sections were collected in 0.1 M PB. Sections from brains containing WGA-HRP or unconjugated HRP were reacted for HRP with 3,3,5,5-tetramethyl benzidine as the chromogen (Mesulam 1978). BDA labeling was revealed using the standard avidin–biotin–peroxidase protocol (Vectastain Elite ABC kit, Vector Laboratories, Burlingame, CA) and 0.01% H_2O_2 in 0.05% 3,3′ diaminobenzidine, with cobalt or nickel intensification; sections were then mounted, dehydrated, defatted, and coverslipped. Tangential sections examined only for the fluorescent tracer RB were mounted on slides and analyzed under epifluorescence without further processing. In some experiments combining WGA-HRP and RB, sections processed for WGA-HRP were often also analyzed for epifluorescence because the fluorescent labeling in these sections was similar to that in sections not processed for WGA-HRP. This allowed a direct correlation of the distribution of RB and WGA-HRP labeling in the same section.

In Situ Hybridization (ISH) for Zif268

In 3 rats, monocular injections of tetrodotoxin (TTX) were administered under general anesthesia induced with a mixture of ketamine (60–90 mg/kg) and xylazine (6–9 mg/kg), and maintained with isoflurane (1–5%). A total volume of 5 μL of TTX (1 mM) was slowly injected into the vitreous of the left eye with a Hamilton Syringe fitted with a glass pipette. Rats recovered and moved freely in their home cages for a period of 24 h, after which time they were anesthetized with ketamine/xylazine followed by an overdose of pentobarbital (120 mg/kg) and perfused intracardially with 4% PFA in 0.1 M PB. The cortical mantles were separated from the brain and flattened. The tissue was postfixed overnight in 4% PFA/30% sucrose/PB at 4°C and cryoprotected in 30% sucrose/PB at 4°C for 1–2 additional nights. Once frozen, the flattened tissue was cut tangentially to the pial surface on a sliding microtome at 40 μm thickness. The sections were kept in a cryoprotectant solution (30% glycerol, 30% ethylene glycol, 40% 0.1 M phosphate-buffered saline) at −20°C.

Preparation of Probes

Plasmids with inserts of specific sequences to rat Zif268 and *ROR*β were prepared with the conventional TA-cloning technique. The sequences of primer sets to clone rat Zif268 were cccaggacaattgaaatttgct (forward) and aaggcaccaagacgtgaaac (reverse), targeting 1878–2678 of NM_001964 including primers. Those for *ROR*β were aaagcaagcacattggagag (forward) and gtcaatgacgtgcccgttgg (reverse), targeting 278–957 of XM_001098940. The sequences were amplified by RT-PCR from rat whole-brain cDNA (Zyagen, San Diego, CA) and inserted into pCR®II-TOPO plasmid vectors (Invitrogen, Carlsbad, CA). Those plasmids were amplified by transfecting into competent cells (*E. coli*) (Invitrogen), and purified. Digoxigenin (DIG)-labeled antisense and sense riboprobes were prepared from the plasmids using a DIG–dUTP labeling kit (Roche Diagnostics, Indianapolis, IN). RNA Probes were then purified with ProbeQuant G-50 Micro Columns (GE Healthcare Life Science, Pittsburg, PA).

Colorimetric ISH

Free-floating sections were soaked in 4% PFA/0.1 M PB (pH 7.4) overnight at 4°C, permeabilized with 0.3% Triton-X for 20 min at room temperature and treated with 3 μg/mL proteinase K for 30 min at 37°C. After acetylation, the sections were incubated in hybridization buffer (5× standard saline citrate [SSC]: 150 mM NaCl, 15 mM Na citrate, pH 7.0), 50% formamide, 2% blocking reagent (Roche Diagnostics), 0.1% *N*-lauroylsarcosine (NLS), 0.1% sodium dodecyl sulfate (SDS), 20 mM maleic acid buffer; pH 7.5] containing 1.0 μg/mL DIG-labeled riboprobe at 60°C overnight. Hybridized sections were washed by successive immersion in wash buffer 1 (2 × SSC, 50% formamide, 0.1% NLS; 60°C, 20 min, twice), RNase A buffer (10 mM Tris–HCl, 10 mM ethylenediamine-*N*,*N*,*N*′,*N*′-tetraacetic acid [EDTA], 500 mM NaCl; pH 8.0) containing 20 μg/mL RNase A (37°C, 30 min), 2 × SSC/ 0.1% NLS (37°C, 20 min) and 0.2 × SSC/0.1% NLS (37°C, 15 min). Hybridization signals were visualized by alkaline phosphatase (AP) immunohistochemical staining using a DIG detection kit (Roche Diagnostics). Sections were mounted onto glass slides, dehydrated through a graded series of increasing ethanol concentrations followed by xylene, and then coverslipped with Permount.

Electrophysiology

Electrophysiological recordings were performed under urethane anesthesia (1200 mg/kg i.p.) supplemented with ketamine (76 mg/kg i.m.). Atropine sulfate (0.1 mg/kg i.p.) was used to reduce tracheal secretion, and dexamethasone (0.001 mg/g s.c.) to prevent brain edema. Body temperature was maintained at 37°C with a heating pad. Pupils were dilated with atropine sulfate ophthalmic solution (1%, Bausch and Lomb), and artificial tears (polyethylene glycol eye drops) and silicone oil were used to protect the corneas and the cerebral cortex, respectively. An area of occipital cortex extending from 2 to 7 mm in the mediolateral direction, and from the lambda suture to 5 mm in the anteroposterior direction was exposed leaving the dura intact. Multiunit activity was recorded with glass-insulated tungsten electrodes (1–2 MΩ; FHC) oriented perpendicularly to the cortical surface at depths of ~400–600 μm. Signals were filtered and amplified with conventional electrophysiological instrumentation, displayed on an oscilloscope and an audio monitor, and stored in a computer. Visual stimuli consisted of hand-held light bars either flashed or swept across the visual field at a distance of 30 cm from the rat's eyes. Each eye was stimulated separately while the nonstimulated eye was covered. Visual responses elicited from an eye ceased when the eye was covered, indicating that covering of the eyes was effective in preventing visual stimulation. Electrode penetrations, spaced at least 200 μm apart, were arranged in a grid over the lateral half of V1. At each recording site, the ocular preference of the multiunit activity was rated on the Hubel and Wiesel's 1–7 scale (Hubel and Wiesel 1962), according to which responses in ocular dominance Group 1 were driven only by the contralateral eye while responses in ocular dominance Group 7 were driven only by the ipsilateral eye. Binocular responses were rated in between, with 4 indicating about equal responsiveness to both eyes.

Two to 3 days prior to recording from one hemisphere, the opposite hemisphere received multiple, evenly spaced injections of HRP to label the pattern of visual callosal connections. In a separate group of rats, HRP was injected intracortically in one hemisphere, and 2–3 days later the splenium of the corpus callosum was transected at the beginning of a recording session on the opposite hemisphere. The splenium was transected by making a parasagittal cut with a #11 scalpel blade in the

hemisphere opposite to the recordings, 1 mm lateral to the midline, 3 mm deep, and extending posteriorly from 3 to 6 mm measured from the bregma suture. Rats with and without callosal transection were perfused immediately at the end of the recording sessions, and the recorded hemispheres were flattened for tangential sectioning. The callosotomy was inspected in coronal sections and only cases with a complete transection of the splenium were analyzed. In 4 rats, cortical cytoarchitecture and visual responsiveness was assessed in the HRP injected hemisphere 2–3 days after the injections. Finally, in 2 additional rats, the splenium was transected *before* the HRP injections, and care was taken to prevent HRP from spilling into the cut. Two days later the animals were perfused and the presence of HRP labeling in both hemispheres was analyzed in coronal sections.

Data Acquisition and Analysis

Identifying the Border of V1 in Anatomical Tracer Experiments

The cytoarchitectonic criteria typically used to identify the border of V1 in coronal sections (Krieg 1946; Caviness 1975; Zilles et al. 1980) cannot be easily applied in tangential sections. We therefore used the myelination pattern, which can be readily displayed in tangential sections. Previous studies show that cytoarchitectonic and myeloarchitectonic criteria for identifying V1 are in close agreement (e.g., Olavarria and Van Sluyters 1984). Before histochemical processing for anatomical tracers, unstained tangential sections were scanned to identify the myelin pattern (Richter and Warner 1974; Laing et al. 2012). In these images, the transition from dense myelination in V1 to reduced myelination at the border of V1 was delineated with the aid of the filter "trace contour" in Adobe Photoshop CS5 (Adobe Systems, CA) (Fig. 1). The myelin pattern was optimally displayed in tangential sections passing through Layer 4 (~500–650 µm deep) and was confirmed in 2 or more sections from the same animal (Fig. 1). Further information for identifying the border of V1 was provided by the relationship that is known to exist between this border and distinct features of the callosal pattern in V1 (Olavarria and Van Sluyters 1985; Laing et al. 2012).

Following histological processing for anatomical tracers, digital images of labeling patterns were obtained by scanning the sections at 2400 dpi using an Epson 4990 scanner. The distribution of callosal cells labeled retrogradely with the fluorescent tracer RB was analyzed using a microscope equipped with a motorized stage (LEPCO) controlled by a Dell XPS T500 computer and a graphic system (Neurolucida, MicroBrightField, Williston, VT). High-magnification images of anatomical tracer labeling or cortical cytoarchitecture were obtained using a DMR Leica microscope coupled to a Leica DC 300F digital camera.

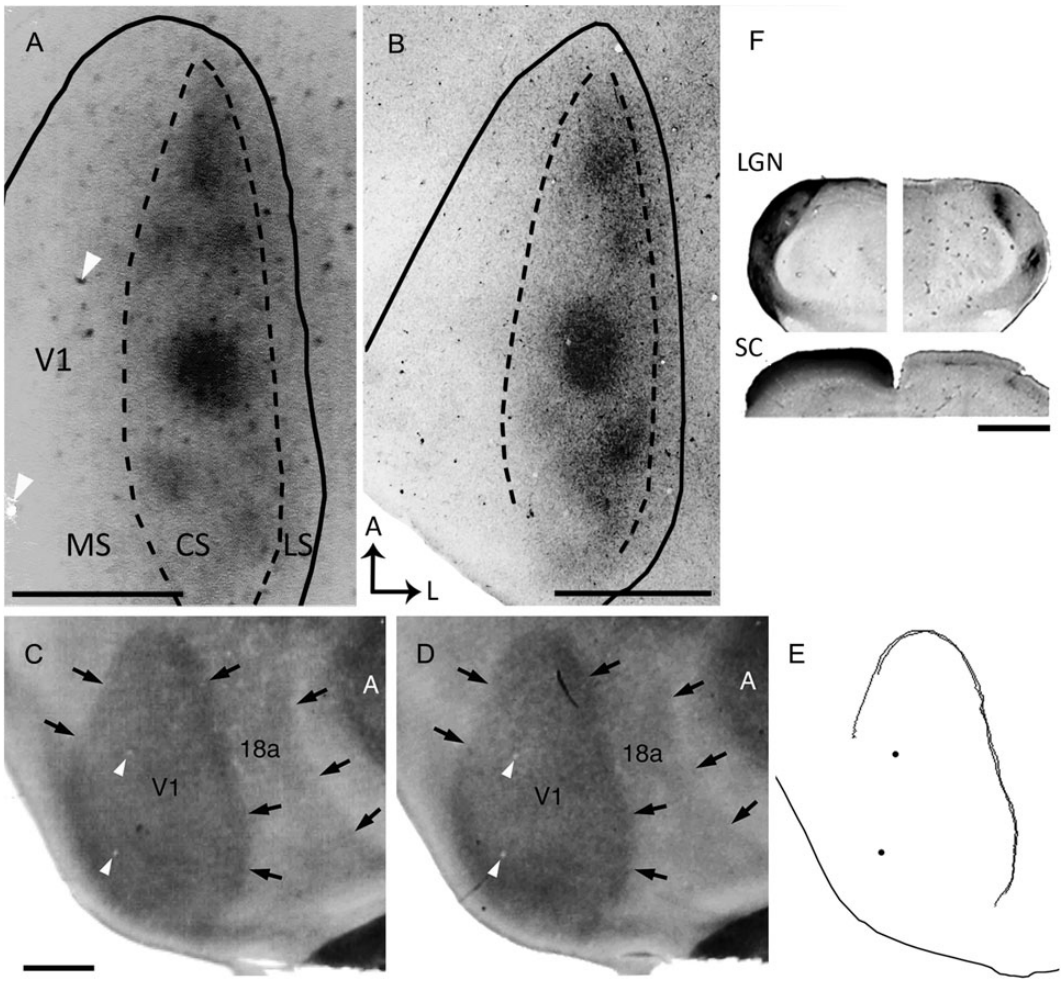

Figure 1. Ipsilateral eye dominance domains in V1 demonstrated by transneuronal transport of WGA-HRP. (*A*,*B*) Tangential sections from 2 rats show dark patches of densely labeled axonal terminations. The black lines indicate the border of V1 as determined from the myelin pattern (see Materials and Methods). Dashed lines delineate the subdivision of V1 into medial (MS), central (CS), and lateral (LS) segments. (*C*,*D*) Myelin patterns from 2 tangential sections taken at the level of Layer 4 (~500 and 540-µm deep, respectively) from case shown in *A*. Arrows indicate the borders of V1 and Area 18a as determined from the myelin pattern. An area of dense myelination corresponding to primary auditory cortex (*A*) is visible lateral to Area 18a. (*E*) Contours of Area V1 delineated from the myelin patterns in *C* and *D* using the filter "trace contour" in Adobe Photoshop (see Materials and Methods). These contours were used to draw the border of V1 in *A*. Black dots mark blood vessels that are also indicated in *A*,*C*,*D* (white arrowheads). Note that panel *A* is slightly rotated clockwise with respect to panels *C*–*E*. (*F*) Subcortical WGA-HRP labeling in case shown in *A*. Coronal sections through the dorsal lateral geniculate nucleus (LGN; top image), and superior colliculus (SC; bottom image) illustrating the contralateral (left), and ipsilateral (right) WGA-HRP labeling patterns. Dorsal is up. Scale bars = 1.0 mm.

Digitized images of anatomical tracer and myelin labeling patterns obtained from each animal were carefully aligned with each other in Adobe Photoshop, using the border of V1, the edges of the sections, radial blood vessels and other fiducial marks as reference. Specific labeling patterns were reconstructed by merging series of carefully aligned neighboring sections. Noise and high pass filters were applied to these patterns to remove gradual changes in staining density across the entire image. Thresholded version of these patterns was then prepared, making sure that they accurately represented the labeling pattern observed in the tissue sections. Quantitative comparisons of anatomical features were evaluated with Student's *t*-test using Bonferroni corrections as needed (significance set at $P < 0.01$). Area measurements were not corrected for potential tissue shrinkage.

The patterns of eye-specific WGA-HRP labeling and callosal connections were reconstructed from series of tangential sections and correlated with each other as described previously (Olavarria 2001). The distribution of callosal labeling was compared with thresholded images of the patterns of eye-specific domains, and the χ^2 test (1 df, significance set at $P < 0.01$) was used to test whether the distribution of callosal connections in both eye-specific domains was different from chance. Counts of RB-labeled cells were estimated by dividing the total pixel count for scored RB cells by the average number of pixels in a single cell. When callosal connections were labeled with BDA, χ^2 was calculated after the analyzed region was divided into 100 equal units.

In the ISH experiments, V1 was identified using the silver procedure for myelin fibers (Gallyas 1979) in a set of tangential sections. The location of Layer 4 was identified by the high expression of *ROR* β mRNA (Hirokawa et al. 2008). Images of myelin and Zif268 expression patterns were captured with a Nikon Eclipse E800M microscope using a high-density CCD color digital camera, DXM1200F (Nikon, Tokyo, Japan). The brightness and contrast of the images were adjusted using Photoshop CS3 Extended (Adobe Systems, CA), and the overall patterns of Zif268 mRNA expression in both hemispheres were reconstructed from 3–5 tangential sections by carefully aligning consecutive sections guided by radial blood vessels and tissue edges.

In the electrode recording experiments, the locations of recording sites with reference to local blood vessels were marked on digital images of the intact cortical surface taken at the beginning of the recording sessions. These images were later correlated with images of the most superficial tangential sections, and the recording sites were matched to the pattern of electrode penetrations observed in these sections. Superficial sections were aligned with deeper sections using the pattern of penetrating blood vessels, section borders, and other landmarks. Following histological processing, the recording sites were assigned to specific regions in V1 that were identified by the patterns of HRP-labeled callosal connections and myelination. Only penetrations judged to be oriented perpendicularly to the cortical surface were analyzed. To evaluate the ocular preference of responses within each of the analyzed regions, a contralateral bias index (CBI) was calculated using the formula:

$$\mathrm{CBI} = [(n1 - n7) + 2/3(n2 - n6) + 1/3(n3 - n5) + N]/2N$$

where N is the total number of recorded sites and nx is the number of sites in an ocular dominance group x. This index ranges from 0.0 to 1.0, values that indicate complete dominance by the ipsilateral or the contralateral eye, respectively. CBIs for the cortical regions analyzed in intact brains were compared using Bonferroni-corrected repeated measures Student's *t*-tests (significance set at $P < 0.01$). CBIs from intact and callosotomized brains were compared using Bonferroni-corrected independent samples Student's *t*-tests (significance set at $P < 0.01$). Figures were prepared using Adobe Photoshop CS5 and all imaging processing used, including contrast enhancement and intensity level adjustments, were applied to the entire images.

Results

Input From the Ipsilateral Eye Forms Separate Patches In Rat Primary Visual Cortex

Our preliminary observation of callosal patches in V1 led us to hypothesize that input from the ipsilateral eye is segregated into specific domains in the rat, and that these domains correlate with callosal patches, as occurs in the cat (Olavarria 2001, 2002). To test whether inputs from the ipsilateral eye form eye-specific domains in V1, we injected WGA-HRP into one eye and examined the resulting pattern of retino-thalamo-cortical input to V1. In the hemisphere ipsilateral to the injected eye, labeling was found in discrete patches located within a restricted portion, ~1.0 mm wide, of V1 (Figs 1*A*,*B*, 2). However, in all cases analyzed, we observed that WGA-HRP labeling was absent or markedly reduced in a narrow strip of cortex, ~0.22 mm in width, that directly adjoined the lateral border of area 17. To aid in the identification of the layer distribution of

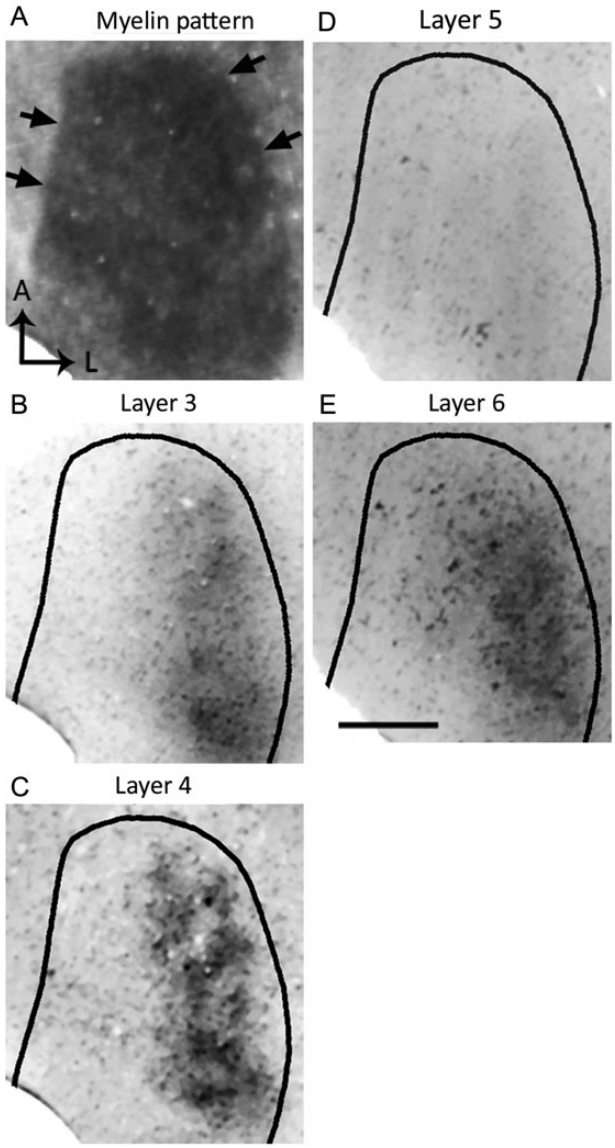

Figure 2. Patterns of transneuronal WGA-HRP labeling at different depths in V1 following an injection of the enzyme into the ipsilateral eye. (*A*) Myelin pattern in section cut at ~540 μm deep. Arrows indicate border of V1. (*B–E*) The pattern of WGA-HRP labeling was most distinct in sections through Layer 4 (*C*, 480 μm) and less distinct in sections through lower Layer 3 (*B*, 360 μm). The pattern was weak or not visible at the level of layer 5 (*D*, 720 μm), but it was again visible in sections through Layer 6 (*E*, 900 μm). The labeling pattern in sections through Layer 6 resembled the pattern observed in sections through Layer 4 suggesting that they are in register. Scale bar = 1.0 mm.

WGA-HRP labeling observed in tangential sections, we also visualized the labeling pattern in coronal sections (see Supplementary Fig. 1) (see also Gerfen et al. 1982; Itaya and Van Hoesen 1982; Kageyama et al. 1990). The WGA-labeling patterns illustrated in Figure 1*A*,*B* are from sections cut at the level of Layer 4, where the pattern is most distinct (see also Fig. 2*C*, see Supplementary Fig. 1). Labeling was also seen in sections through lower layer 3 (Fig. 2*B*, see Supplementary Fig. 1), but the pattern was less distinct. In deeper sections, the pattern was weak or not visible at the level of Layer 5 (Fig. 2*D* and see Supplementary Fig. 1), but it was again visible in sections through Layer 6 (Fig. 2*E* and see Supplementary Fig. 1). The labeling pattern in sections through Layer 6 resembled the pattern observed in sections through Layer 4 (cf. Fig. 2*C*,*E*), suggesting that patterns of geniculate input to both layers are in register with each other, as occurs in the cat (LeVay and Gilbert 1976).

Tripartite Subdivision of V1

Based on the pattern of ipsilateral transneuronal WGA-HRP labeling described above, we recognized 3 main subdivisions within V1: 1) The Central Segment (CS), defined as the area containing the ipsilateral eye-specific domains (outlined by dashed lines in Fig. 1*A*,*B*). We estimate that the surface area occupied by ipsilateral eye domains is about one-third of the total surface area of the CS (see below). 2) The medial segment (MS), located medial to the CS, presumably represents the peripheral monocular visual field. 3) The lateral segment (LS), located between the CS and the lateral border of V1.

Examination of WGA-HRP labeling in the superior colliculus (SC) and dorsal lateral geniculate nucleus (dLGN) showed the typical patterns of retinal projections to these nuclei in the rat (Fig. 1*F*). Ipsilateral to the injected eye, labeling was restricted to one or more densely labeled patches in dorsomedial regions of the dLGN, while contralaterally the labeling was uniformly dense throughout the dLGN, except for a small dorsomedial region that presumably corresponds to the ipsilateral eye recipient zone. Similarly, weak, patchy input was seen in the ipsilateral SC, while dense, uniform labeling occupied the contralateral SC. These observations make it unlikely that the patchy distribution of ipsilateral eye input in V1 is due to obvious anomalies in retino-thalamic projections, or incomplete or uneven uptake of the tracer by retinal ganglion cells.

Patchy Callosal Connections In Rat Primary Visual Cortex

Previous studies report that the distribution of callosal connections in visual cortex peaks at the border region between areas 17 and 18a and extends some distance into these areas (e.g., Cusick and Lund 1981; Olavarria and Van Sluyters 1985). However, in preliminary experiments we observed that callosal connections in V1 are often markedly inhomogeneous in the tangential plane. In the present study we carefully examined the distribution of callosal cells and fibers in V1 as revealed by multiple, evenly spaced intracortical injections of several anatomical tracers, including HRP (Fig. 3*A*,*B*, Supplementary Fig. 2*A*), BDA (Fig. 3*C*), or RB (Supplementary Fig. 2*B*). We observed that, independent of the tracer used, 2 callosal regions could be readily recognized in tangential sections through Area V1 in the hemisphere opposite to the injections: a medial callosal region, ~1.0 mm wide at the widest part, where callosal connections typically formed distinct, densely labeled patches of different shapes and sizes (arrows in Fig. 3*A*–*C*), and a lateral region, indicated by the dashed line in Figure 3*A*–*C*, where callosal connections form a band ~0.22 mm wide abutting the border of V1. In most rats examined, this band was homogeneously labeled throughout its anteroposterior extent, but occasionally the labeling was less dense at one or 2 discrete sites. By its location and width, the lateral callosal band corresponds closely with the LS described above (cf. Figs 1 and 3; see below). In agreement with previous descriptions of the laminar distribution of labeled callosal connections (e.g., Olavarria and Van Sluyters 1985), we observed that the callosal pattern was apparent in tangential sections through Layers 2–6, although it appeared somewhat sharper at depths that likely correspond to Layer 4 (~500 µm deep). The patchy appearance of the callosal pattern in tangential sections is not likely due to incomplete or uneven infiltration and transcallosal transport of the tracers because the dLGN ipsilateral to the cortical injections was uniformly labeled with the tracer used in the experiments (see Supplementary Fig. 3*A*).

As noted above, both the patchy medial region and the lateral band were observed in the patterns of callosal labeling regardless of the tracer used. At higher magnification, retrogradely labeled somas and dendritic branches were observed with HRP (Fig. 3*D*–*G* and Supplementary Fig. 2*A*), retrogradely labeled somas were observed with RB (see Supplementary Fig. 2*B*), while dense networks of labeled fibers, likely including axonal fibers and terminations, and some dendritic branches, were observed with BDA (Fig. 3*H*). These observations are in agreement with previous descriptions of the transport properties of HRP (Trojanowski et al. 1981), BDA (Reiner et al. 2000), and RB (Katz et al. 1984), and confirm that regions giving rise and receiving visual callosal connections are in close spatial register in Rat V1 (e.g., Cusick and Lund 1981; Olavarria and Van Sluyters 1985).

Ipsilateral-Eye Domains Correlate With Callosal Patches In Rat V1

The pattern of ipsilateral eye domains resembled the pattern of callosal patches in the medial callosal region. Patches of ipsilateral eye input and of callosal connections tended to be circular or oval in shape, and often the largest patches were located at midanteroposterior levels (Figs 1 and 3). However, more complex shapes that sometimes appeared to be formed by the fusion of nearby patches were also observed. Callosal and ipsilateral eye patches were arranged anteroposteriorly into either single or double strings of patches (Figs 1, 3 and 5).

To assess the similarity between patches of callosal connections and of ipsilateral eye input quantitatively, we measured the size and number of callosal patches and ipsilateral eye domains in different group of rats. On average, ipsilateral eye domains analyzed in 7 rats measured 0.12 mm^2 (SEM = 0.0082 mm^2) in size, and their number ranged from 7 to 12 (M = 9.3, SEM = 0.81). Callosal patches analyzed in 7 rats measured 0.12 mm^2 (SEM = 0.0084 mm^2) in size and their number ranged from 6 to 12 (M = 8.0, SEM = 0.76). We found no significant differences between ipsilateral eye domains and callosal patches when size of patches ($P = 0.68$) and number of patches ($P = 0.27$) were compared across groups (Fig. 4*A*,*B*, respectively). Furthermore, when the surface area occupied by ipsilateral eye domains (33.9 ± 0.06%) and callosal patches (34.6 ± 0.02%) was

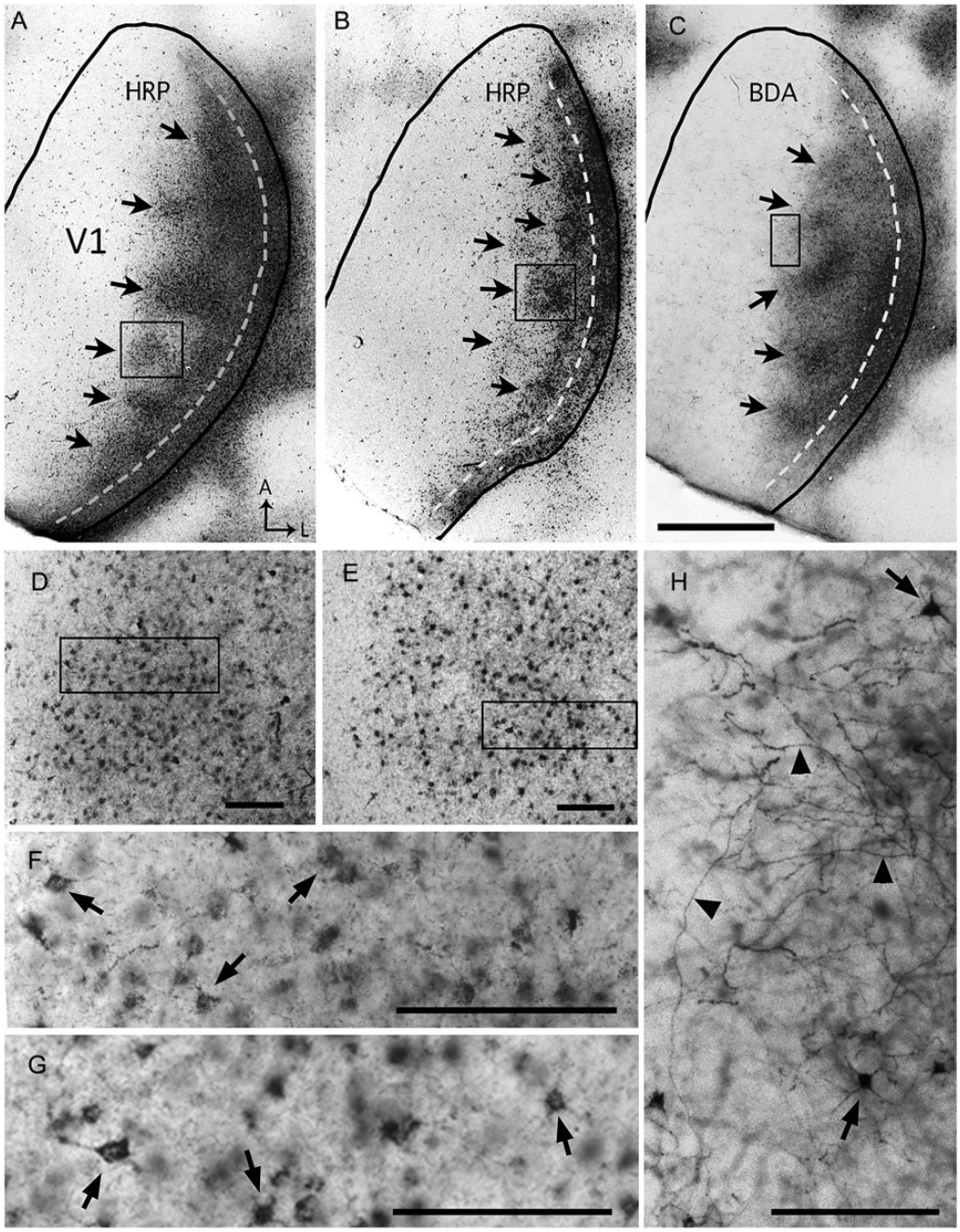

Figure 3. Patchy callosal connections demonstrated in tangential sections through the right V1 following multiple intracortical injections of HRP (*A*,*B*) or BDA (*C*) into the left hemisphere. The black lines indicate the border of V1. Dark areas in lateral V1 correspond to dense accumulations of transported tracer. This labeled callosal region consists of a series of patches located medially (arrows in *A*–*C*) and a densely labeled band adjacent to the lateral border of V1 (dashed lines in *A*–*C*). Panels *D* and *E* are higher-magnification views of the callosal patches within the boxes in *A* and *B*, respectively, and the boxes in *D* and *E* are shown at higher magnification in *F* and *G*, respectively. Higher-magnification views of HRP-labeled regions show primarily retrogradely labeled somas (dark dots in *D* and *E*) and finer labeling likely contained in axons and dendrites (Trojanowski et al. 1981). Arrows in *F* and *G* indicate retrogradely HRP-labeled somas. Panel *H* is a high-magnification view of the BDA-labeling within the box in *C*, and it illustrates that BDA (10 kDa) primarily labels fibers (black arrowheads) that likely transported BDA anterogradely, and occasionally somas and dendrites (arrows) (Reiner et al. 2000). *A*: anterior, *L*: lateral. Scale bar in *C* = 1.0 mm; in *D*–*H* = 100 μm.

compared in the CS (Fig. 4*C*), no significant difference was observed ($P = 0.96$).

To test the hypothesis that ipsilateral eye domains are spatially correlated with callosal patches, we labeled both projections in the same animal. Figure 5 illustrates results from 2 animals that received an intraocular injection of WGA-HRP into the right eye, and intracortical injections of either RB (Fig. 5*A*–*D*) or BDA (Fig. 5*E*–*H*) into the left hemisphere. In the first case, the pattern of ipsilateral eye-specific domains is shown in panels *A* and *B*, while the pattern of callosal connections labeled with RB is shown in panel *C*. These patterns are superimposed in panel *D*, with the areas of overlap colored yellow. Similarly, in the second case Panels *E* and *F* show the ipsilateral eye-specific domains, and panel *G* shows the pattern of callosal connections labeled with BDA. Panel *H* shows the superimposition of both patterns, with the areas of

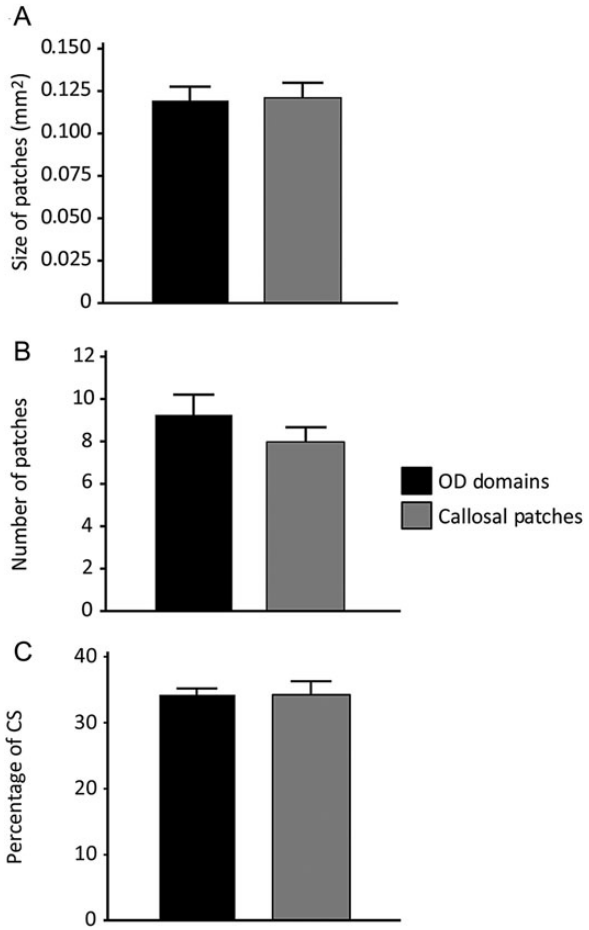

Figure 4. Comparison of callosal patches and ipsilateral eye domains. (*A*) Size of callosal patches demonstrated with intracortical injections of tracers and ipsilateral eye domains demonstrated with intraocular injections of WGA-HRP in different groups of rats ($N = 7$ per group). Mean sizes (and SEM) were calculated by measuring the area of labeled regions in thresholded versions of the labeling patterns demonstrated in tangential sections. (*B*) Comparison of the number (mean ± SEM) of ipsilateral eye domains and callosal patches within the CS. (*C*) Percentage of the surface area of CS that is occupied by ipsilateral eye domains and callosal patches. No significance was found when the size of patches, number of patches and the percentage of the CS occupied by the patches were compared between the 2 groups ($P > 0.01$).

overlap colored yellow. In both rats, callosal patches were significantly correlated with ipsilateral eye-specific domains in the areas analyzed (outlined by dashed gray lines in Fig. 5*D*, *H*) (χ^2, $P < 0.01$). Note that the area analyzed excludes the LS, where callosal connections typically form a homogeneous band. Similar results were obtained in 2 other rats in which callosal connections were studied following multiple injections of RB (χ^2, $P < 0.01$). These results show that callosal patches are in spatial correlation with the ipsilateral eye domains, as it occurs in the cat (Olavarria 2001). In addition, they show that the lateral, homogeneously labeled band of callosal connections overlaps with the LS (indicated by the black dashed line in Fig. 5).

Areas of Reduced Contralateral Eye Input In V1 Correlate With Callosal Patches

We next investigated whether contralateral eye input to the CS occupies territories that are complementary to, and interdigitated with, the ipsilateral eye domains. If so, one would expect that contralateral eye input would be reduced or absent in areas of ipsilateral eye input. Moreover, since ipsilateral eye domains overlap with callosal patches, areas of reduced contralateral eye input should also correlate with patches of callosal connections.

Contralateral WGA-HRP labeling was densely distributed throughout V1 except for small areas of reduced labeling in the CS ($n = 3$). Further, intracortical injections of tracers in the opposite hemisphere of the same animals revealed that the areas of reduced contralateral labeling were significantly correlated with patches of callosal input. Figure 6 illustrates results from the right hemisphere of an animal that received an intraocular injection of WGA-HRP into the left eye, and intracortical injections of BDA into the left hemisphere. Areas of reduced contralateral eye input (Fig. 6*A*) are outlined in green in Figure 6*B*, while BDA-labeled callosal regions in the same hemisphere are shown in Figure 6*C* (red outline). In Figure 6*D*, the outline of the callosal pattern (red line) is superimposed to a thresholded representation of the pattern of WGA-HRP labeling, in which the areas of reduced labeling appear white. Analysis of these data shows that callosal patches are significantly correlated with areas of reduced contralateral eye input in the CS (χ^2, $P < 0.01$). Plots of the labeling density (Fig. 6*E*) show that the increase in the density of callosal labeling (red trace) corresponds precisely with a reduction of input from the contralateral eye (green trace). These results provide anatomical evidence of partial segregation between contralateral and ipsilateral eye input in the CS. In addition, they show that the LS receives strong input from the contralateral eye, and confirm data in Figure 5 illustrating that the LS overlaps with a dense band of callosal connections in lateral V1.

In summary, our anatomical data provide evidence that the CS receives largely segregated input from both eyes, while the MS and LS are exclusively or primarily innervated by direct projections from the contralateral eye. In addition, our analysis of the correlation between retino-thalamo-cortical projections and callosal connections indicates that callosal patches in the CS overlap with ipsilateral eye domains, while the lateral callosal band overlaps with contralateral eye input to the LS.

Functional Segregation of Contralateral and Ipsilateral Eye Domains in V1 Demonstrated With ISH for Zif268

Do the patterns of eye-specific inputs demonstrated anatomically result in neural responses in V1 that are also eye-specific? We addressed this question by analyzing the patterns of expression of the immediate early gene Zif268, which is rapidly and transiently induced by neuronal activity (Sheng and Greenberg 1990; Chaudhuri et al. 1995, 1997; Markstahler et al. 1998; Caleo et al. 1999; Horton et al. 2000; Takahata et al. 2009, 2014; van Brussel et al. 2009). Previous analysis of Zif268 mRNA expression after monocular inactivation with either intraocular injections of TTX, monocular deprivation or enucleation have revealed Zif268 activation patterns that closely resemble the patterns of ODCs demonstrated with anatomical methods (e.g., Chaudhuri et al. 1995, 1997; Horton et al. 2000; Takahata et al. 2009, 2014). We therefore used Zif268 induction to map functional activation driven by each eye in V1 and compared the resulting maps with anatomical patterns of geniculocortical projections. Studies using coronal sections have reported that the basal expression of Zif268 is relatively high in V1 of normally behaving rats, and that labeling is visible in all layers, except Layer 1, but most

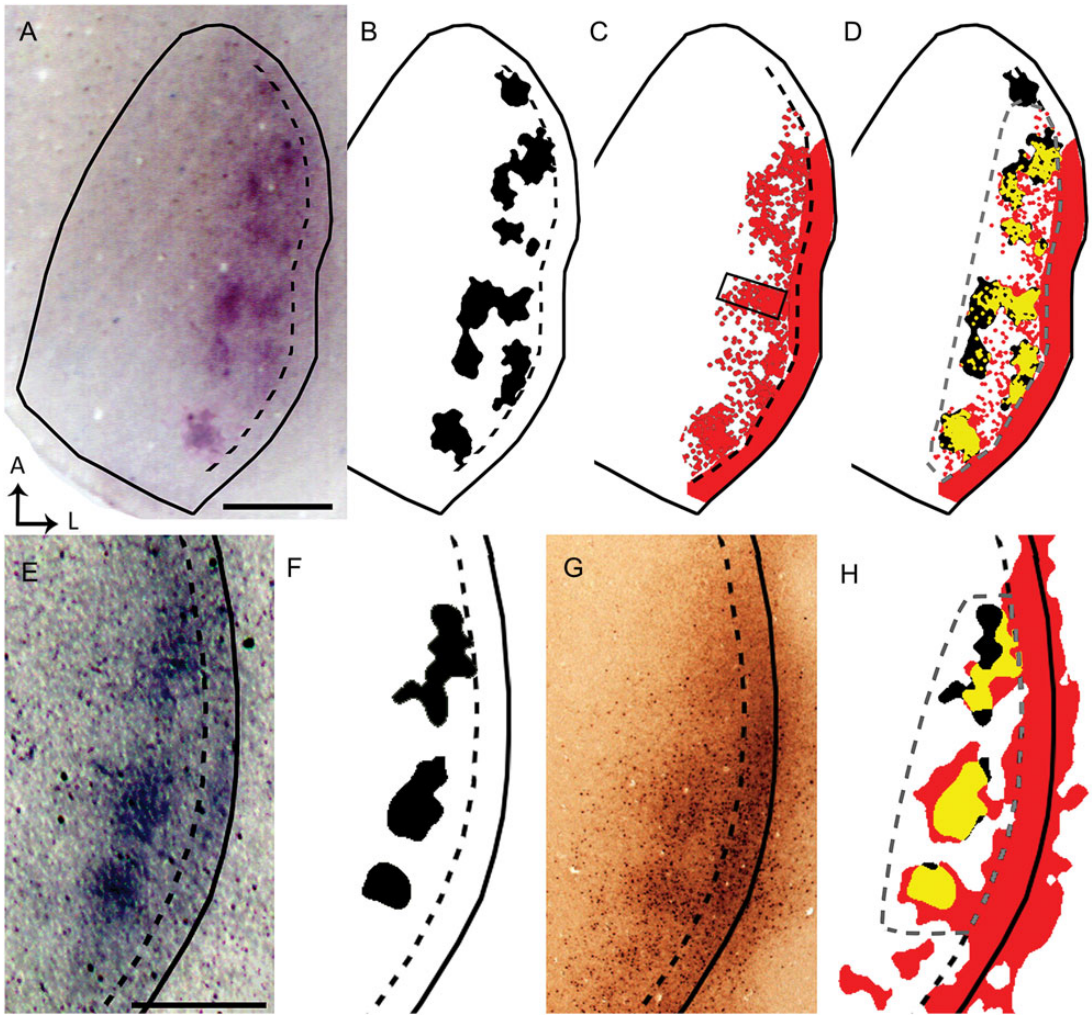

Figure 5. Data from 2 rats (*A–D* and *E–H*) illustrate that ipsilateral eye domains correlate with callosal patches in the same animal. Solid black lines indicate the border of V1. Dashed black lines indicate estimated border between the CS and LS. WGA-HRP-labeled ipsilateral eye domains (*A*,*E*; thresholded version shown in black in *B* and *F*, respectively) were correlated in the same animal with callosal connections demonstrated with RB (red areas in *C*) or with BDA (*G*, thresholded version colored red in *H*). High-magnification images captured under epifluorescence of the callosal patch within the box in *C* show RB-labeled cells bodies (see Supplementary Fig. 2*B*), illustrating that this tracer is transported retrogradely (Katz et al. 1984). In *D* and *H*, the patterns of callosal connections are shown superimposed to the patterns of ipsilateral eye domains from the same animal, and the overlapping regions are colored yellow. Statistical analysis of the correlation was performed in the area outlined by the dashed gray line in *D* and *H* (χ^2, $P < 0.01$). Scale bars = 1.0 mm.

prominently in Layers 4 and 6 and least densely in Layer 3 and 5 (Schlingensiepen et al. 1991; Caleo et al. 1999).

In 3 rats, TTX was injected into one eye to down regulate the expression of Zif268 mRNA in territories innervated by that eye. We observed a striking similarity between the patterns of Zif268 activation within V1 and the distribution of eye-specific domains revealed by the transneuronal transport of WGA-HRP (cf. Figs 1 and 7*B*). In the hemisphere ipsilateral to the active eye (Fig. 7*B*), strong Zif268 activation was restricted to a number of distinct, densely labeled patches resembling those revealed by WGA-HRP labeling. The size of Zif268 patches measured in 3 rats was not significantly different from the size of patches labeled with WGA-HRP ($P = 0.46$). Moreover, patches labeled by the 2 methods were restricted to the CS.

Equally striking was the similarity between the Zif268 staining pattern observed in the hemisphere contralateral to the active eye and the pattern of WGA-HRP transport from the contralateral eye. Here, the pattern of Zif268 activation was strong throughout V1 except in a number of small patches in the CS that, judging by their location and number, likely correspond to regions innervated by the inactivated ipsilateral eye (Fig. 7*A*). In both hemispheres, the patterns of Zif268 labeling in V1 were more distinct at the levels of Layer 4 (Fig. 7*F*) and 6 (Fig. 7*H*) than at the levels of Layers 2–3 (Fig. 7*D*) and 5 (Fig. 7*G*). Finally, consistent with previous studies in normal rats (Caleo et al. 1999), in a control animal we observed a strong and homogenous pattern of Zif268 throughout V1, without obvious periodicity in labeling density (Fig. 8). The sense probes detected no signals stronger than background (Fig. 8B).

It is interesting to note that while the active eye induced strong Zif268 expression in the contralateral LS (Fig. 7*A*), it failed to induce obvious Zif268 expression in the ipsilateral LS (Fig. 7*B*). These results were unexpected because they suggest that the binocular zone does not extend to the lateral border of V1 as is commonly believed. Instead, our results provide evidence that the LS in hooded rats is predominantly monocular.

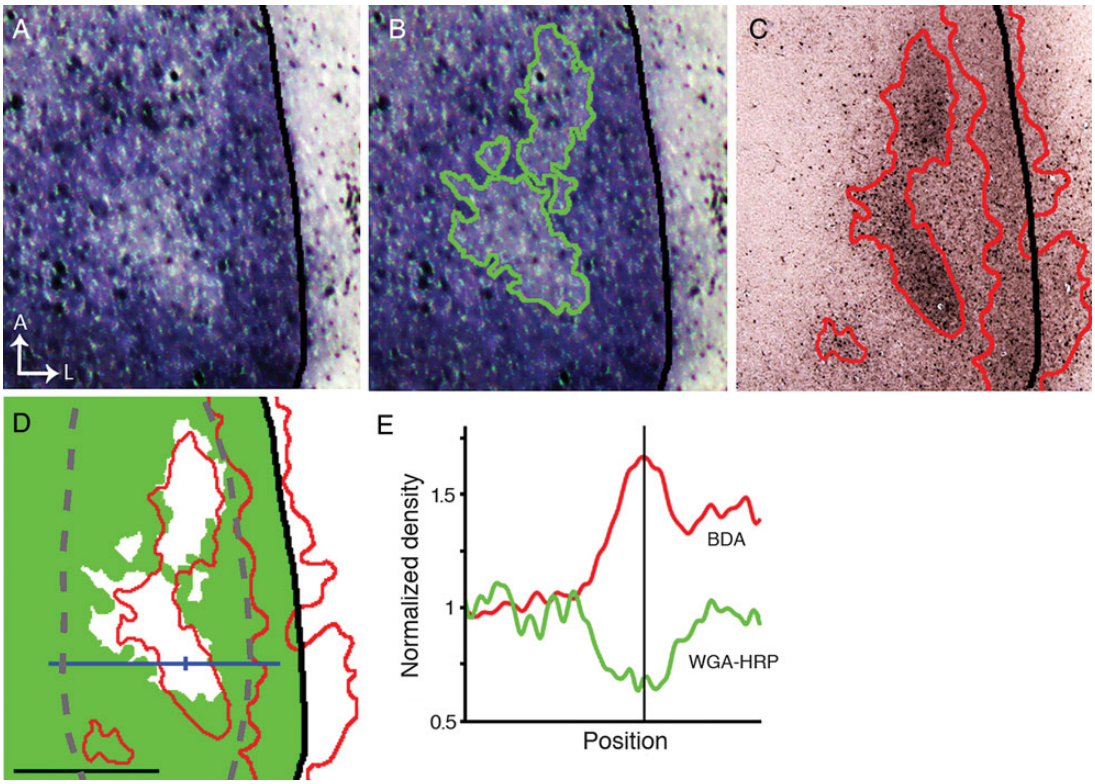

Figure 6. Areas of reduced contralateral eye input in V1 correlate with callosal patches. (*A*) Areas of reduced WGA-HRP labeling in the hemisphere contralateral to the eye injected with WGA-HRP. (*B*) The green line outlining these areas was determined by thresholding the labeling pattern in *A*. (*C*) Pattern of callosal connections in the same animal demonstrated by multiple intracortical injections of BDA in the opposite hemisphere. Densely labeled callosal regions are outlined by red lines determined by thresholding the image. (*D*) The outline of the callosal pattern (red line) is shown superimposed to a thresholded version of the WGA-labeling pattern in *B*, in which densely labeled areas are colored green while the areas of reduced WGA-labeling appear white. Note that only callosal patches in the CS correlate with areas of reduced WGA-HRP labeling. Statistical analysis of the correlation was performed in the area outlined by the dashed gray line (χ^2, $P < 0.01$). The area occupied by the densely labeled band of callosal connections at the LS receives strong input from the contralateral eye. (*E*) Plots of the labeling density at the level indicated by the blue line in *D* show that the increase in the density of BDA callosal labeling (red curve) corresponds precisely with a reduction of input from the contralateral eye (green curve). The vertical line in *E* corresponds to the tick mark on the blue line in *D*. Scale bar = 1.0 mm.

Electrophysiological Mapping of Ocular Dominance Preference in Normal and Callosotomized Rats

Our analysis of the patterns of Zif268 activation in rats monocularly injected with TTX suggests that the functional patterns of eye-specific representation in V1 are relayed through eye-specific projections demonstrated with WGA-HRP. However, we showed that callosal patches colocalize with ipsilateral eye domains revealed with WGA-HRP, and that the LS overlaps with a dense, homogeneous band of callosal connections. An obvious question is whether both the ipsilateral eye-driven activity observed in the CS and the contralateral eye-driven activity observed in the LS are relayed through the callosum, rather than through direct retino-thalamo-cortical projections. We addressed this question by recording visual responses in V1 electrophysiologically, both in intact rats and in rats that underwent callosotomy at the beginning of the recording session (see Materials and Methods).

In both intact and callosotomized rats, electrode penetrations orthogonal to the brain surface were arranged in a grid over the lateral half of V1. The multiunit activity driven by visual stimulation of each eye was compared at each site and the ocular preference was rated on the Hubel and Wiesel's 1–7 scale (Hubel and Wiesel 1962). Two or 3 days prior to the recordings, these rats received intracortical injections of HRP in order to label the callosal connections in the recorded hemisphere. This allowed correlating the electrode penetrations with eye-specific regions identified in the callosal pattern in V1. Intraocular injections of WGA-HRP were not used to identify these regions in order to avoid the risk of retinal damage, which could have interfered with the recording of evoked responses from the injected eye.

In both experimental groups, electrode penetrations were assigned to one of 3 groups. In the CS, penetrations that were located outside callosal patches were grouped as "interpatch", penetrations that were located within callosal patches were grouped as "on patch". The third group consisted of penetrations that fell within the LS. Penetrations that could not be assigned to one of these regions with certainty were not included. Figure 9*A*,*B* illustrates an experiment performed in a rat with intact callosum, in which the location of recording sites (white, black dots in *A*, *B*, respectively) were identified with reference to the callosal pattern in the same animal. These data illustrate that penetrations within patches tended to have higher Hubel and Wiesel scores (stronger ipsilateral eye responses) than those falling either between patches or within the LS.

Data pooled from all penetrations assigned to each cortical region show that in both intact and callosotomized rats the binocularity assessed using the scale of Hubel and Wiesel (1962) changed markedly depending on the region that was recorded

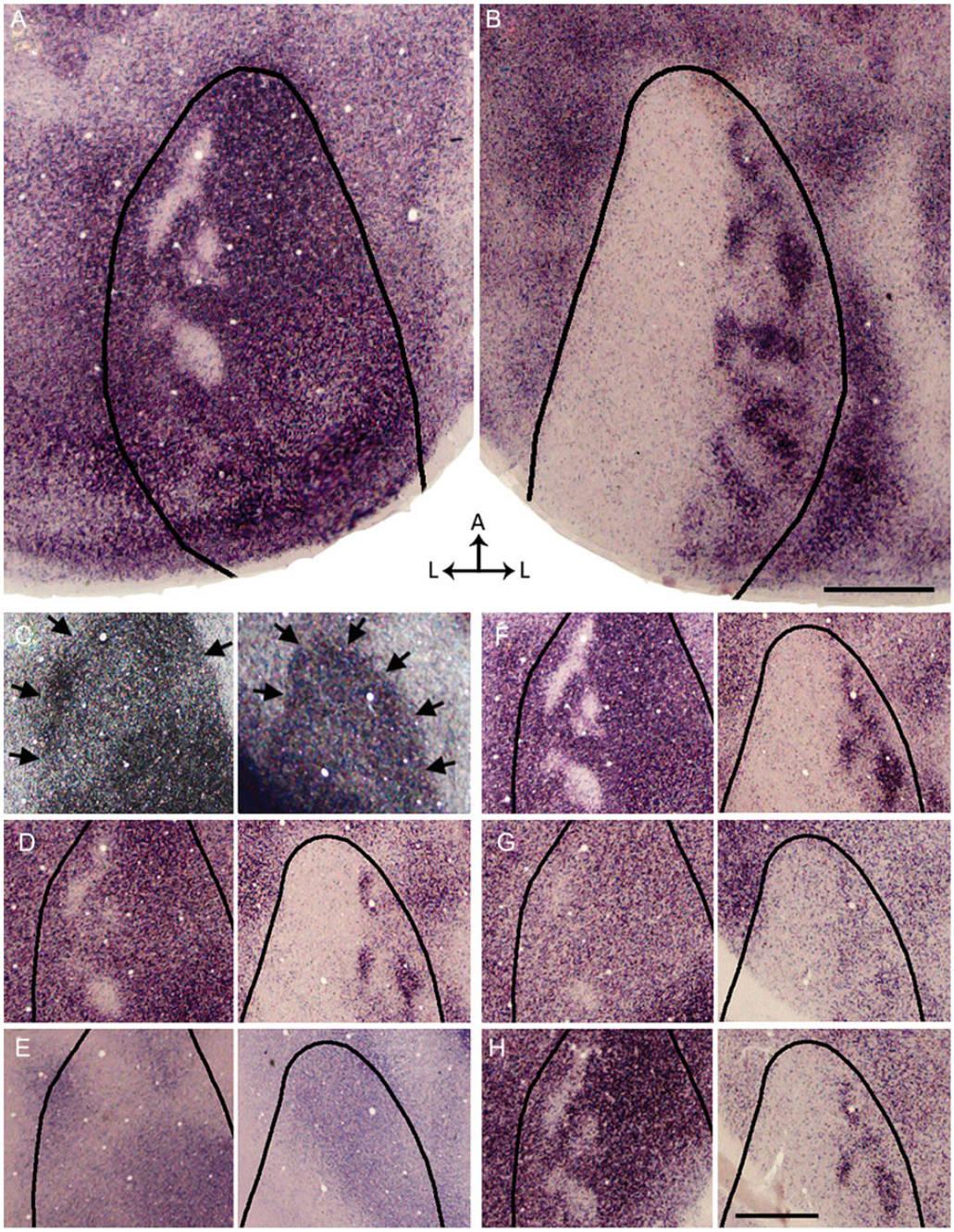

Figure 7. Functional segregation of contralateral and ipsilateral eye domains in V1 demonstrated with ISH for Zif268 after an injection of TTX into the left eye, leaving only the right eye active. (*A*,*B*) Overall patterns of Zif268 expression in the left (*A*) and right (*B*) hemispheres reconstructed from 3 and 4 tangential sections, respectively. Areas of strong Zif268 expression, corresponding to activity driven by the right eye, appear darkly stained. In the left V1 (*A*), pale patches presumably correspond to domains innervated by the silent left eye. In the right V1 (*B*), dark patches presumably correspond to domains driven by the active right eye. The black outlines indicate the border of V1 as revealed in the myelin pattern. (*C*–*H*) Left and right images in each pair are from the left and right hemispheres, respectively. (*C*) Pattern of myelination used to determine the border of V1 (arrows). The complete myelination patterns for V1 were available for delineating the border of V1 in *A*,*B*. (*D*) Pattern of Zif268 expression in supragranular layers. (*E*) Pattern of ROR β labeling in section through Layer 4 (Hirokawa et al. 2008). (*F*) Pattern of Zif268 expression is strongest at the level of Layer 4, immediately below the section stained for ROR β (*E*). (*G*) The pattern of Zif268 expression weakens and becomes less discernible at approximately the level of Layer 5, but it becomes stronger in sections through Layer 6 (*H*). Scale bars = 1.0 mm.

(Fig. 9*C*,*D*). These data were analyzed by comparing the CBIs for each region in both intact and callosotomized rats (Fig. 9*E*). Consistent with our functional analysis using ISH for Zif268 (Fig. 7), in intact rats we found that CBIs were significantly higher on interpatch (M = 0.88, SEM = 0.02, $n = 12$) and LS (M = 0.93, SEM = 0.03, $n = 9$) regions when compared to CBIs for patches (M = 0.51, SEM = 0.04, $n = 11$) ($P < 0.01$, Bonferroni-corrected repeated measures Student's *t*-tests). No significant differences were found between the interpatch region and LS ($P > 0.01$). In callosotomized rats we found that the region-specific CBIs (interpatch: M = 0.85, SEM = 0.05, $n = 7$; LS: M = 0.96, SEM = 0.02, $n = 9$; patch: M = 0.51, SEM = 0.03, $n = 12$) were no significantly different from the corresponding values in intact rats ($P > 0.01$, Bonferroni-corrected independent

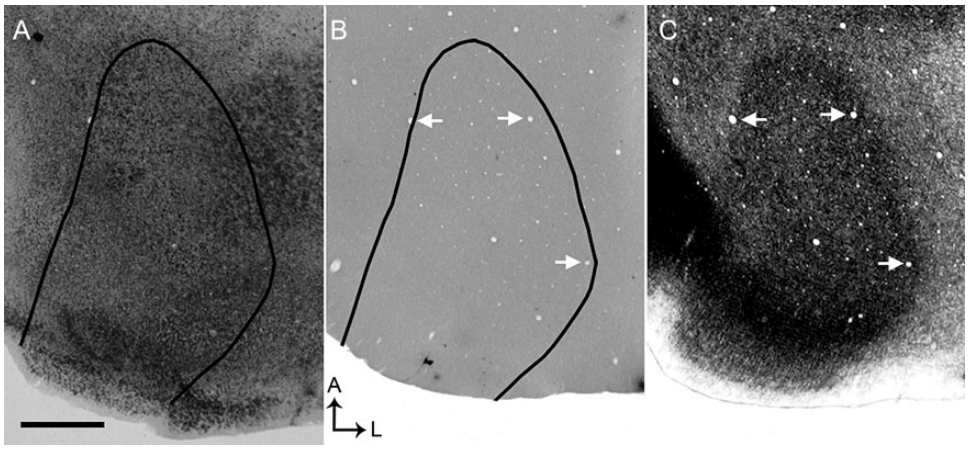

Figure 8. Pattern of Zif268 expression in visual cortex of control rat. (*A*) Overall pattern of Zif268 expression in the right hemisphere reconstructed from 4 tangential sections. A strong and homogeneous pattern of Zif268 expression is observed throughout V1, without obvious patchiness in labeling density. (*B*) ISH with the sense probes yielded no signals stronger than background. The black outlines in (*A*) and (*B*) indicates the border of V1 as visualized in a tangential section stained for myelin (*C*). Arrows point to the same blood vessels in *B* and *C* to facilitate the correlation of the V1 border in *B* with the myelin pattern in *C*. Scale bar = 1.0 mm.

samples Student's *t*-tests). These results provide evidence that the ocular dominance preference assessed within callosal regions in the CS and LS does not depend primarily on activity relayed through the callosal commissure.

A possible confound of our callosotomy test is that the HRP injections may cause extensive cortical damage, essentially obliterating callosal input to the recorded hemisphere in the control group. To address this possibility, we examined the cytoarchitecture of V1 and cell responsiveness in 4 rats that received multiple, evenly spaced injections of HRP in visual cortex of one hemisphere. Recording from lateral V1 in the injected cortex was performed 2–3 days following the HRP injections. HRP labeling in the contralateral hemisphere and ipsilateral thalamus was revealed as in the experiments described above. We observed that cytoarchitectonic changes produced by the HRP injections were restricted to the injection tracks, without obvious changes in the surrounding cortex. Moreover, in all 4 rats stimuli-evoked cell responses in lateral V1 were comparable in strength to responses recorded from lateral V1 in a rat not injected with HRP (see Supplementary Fig. 3). These observations provide evidence that visual responsiveness was maintained in the HRP injected hemisphere.

In 2 additional rats, the splenium was transected *before* the intracortical injections of HRP. Strong HRP labeling was present in the cortex, thalamus and superior colliculus of the injected hemisphere, while no labeling was observed in visual cortex of the opposite hemisphere (Fig. 9*F*), confirming the effectiveness of our procedure for transecting the callosal commissure. No physiological data were collected from these 2 rats.

Discussion

Using a combination of anatomical tracers we have demonstrated clear patchiness in the distribution of eye-specific retino-thalamo-cortical projections and callosal connections in V1 of Long Evans rats. Moreover, we found that eye-specific and callosal patches bear a systematic relationship with each other, as well as with functional representations of each eye assessed with both ISH for Zif268 expression and electrophysiological methods. Although recordings within ipsilateral eye domains in V1 had significantly higher Hubel and Wiesel scores (stronger ipsilateral eye responses) than those falling either between patches or within the LS, sites exclusively dominated by the ipsilateral eye were relatively uncommon within ipsilateral domains (Fig. 9). These observations suggest that, as in the cat (Hubel and Wiesel 1962; Shatz et al. 1977), input from both eyes may overlap to some extent in Layer 4. In the rat this overlap may be more evident for penetrations within ipsilateral eye domains due to the small size of these domains compared with the size of contralateral eye domains within the CS.

Previous Studies in Rodents and Ferrets

Previous studies in rats using transneuronal techniques have not described eye-specific domains possibly because they sectioned the brain in the coronal plane, an approach that is not optimal for detecting the relatively small periodicities we describe (Gerfen et al. 1982; Itaya and Van Hoesen 1982; Itaya 1988; Kageyama et al. 1990). Moreover, most of these studies did not use Long Evans rats. Although the existence of cortical patches dominated by one eye has been suggested in studies using physiological techniques (Caleo et al. 1999) or changes in glucose metabolic activity (Thurlow and Cooper 1988), these studies were not primarily focused on this issue and did not attempt to demonstrate eye-specific segregation with anatomical methods. Caleo et al. (1999) revealed the pattern of Zif268 immunostaining in rat visual cortex after monocular injections of TTX, but they do not report the existence of patchy staining in the binocular region, possibly because they displayed the labeling data as revealed in single coronal sections. Finally, a small-scale (<100 μm) honeycomb pattern has been described at the Layer 1–2 border in visual cortex of Wistar albino rats (Ichinohe et al. 2003), but its relationship with the patterns of thalamic or callosal projections described here, if any, remains to be investigated.

In mice, no cortical organization related to ocular dominance has been reported by studies using various techniques (Dräger 1974; Antonini et al. 1999; Kalatsky and Stryker 2003; Mrsic-Flögel et al. 2007; van Brussel et al. 2009). However, a study in knockout mice lacking the transmembrane glycoprotein

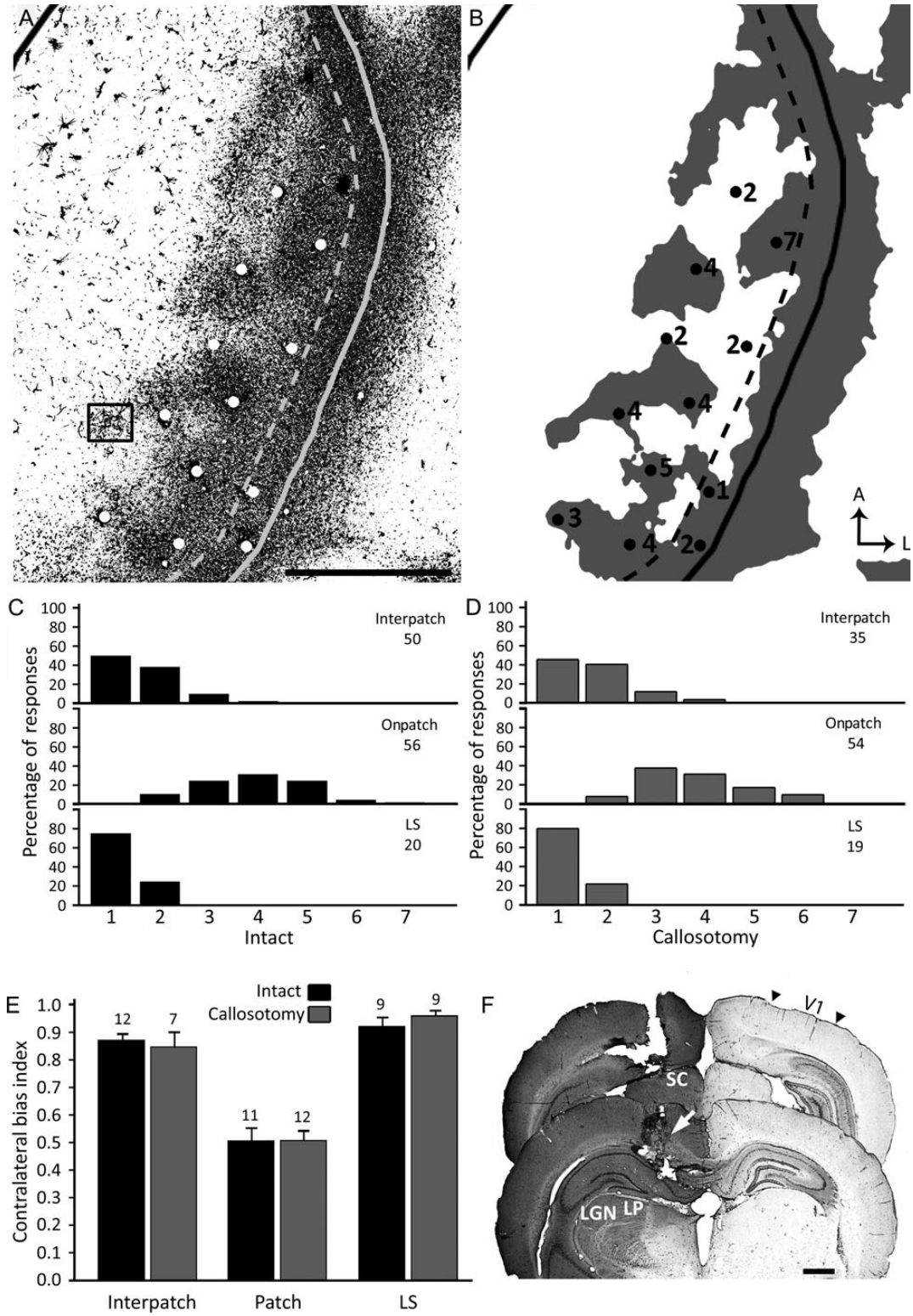

Figure 9. Electrophysiological mapping of ocular dominance preference in intact and callosotomized rats. (*A*) Pattern of callosal connections in the right V1 demonstrated after multiple injections of HRP into the opposite hemisphere in an intact rat. HRP-labeled cells in the region indicated by the box are shown at higher magnification in Supplementary Figure 2*A*. Speckles in medial regions of V1 represent reaction artifact. (*B*) Thresholded version of the callosal pattern. The dashed line in *A* and *B* indicates the approximate border between the CS and the LS, while the solid line indicates the border of V1. Dots in *A* and *B* indicate electrophysiological recording sites in the same animal. In *B*, the Hubel and Wiesel rating for ocular preference is indicated by the number next to the penetrations. (*C*,*D*) Recording sites were classified into 3 groups depending on whether they fell on a patch or interpatch regions of the CS, or within the LS. The histograms represent the percent of sites assigned to each of the 7 Hubel and Wiesel ocular dominance classes in each of these regions in intact (*C*) and callosotomized rats (*D*). The number of sites recorded in each region is indicated. (*E*) Comparison of contralateral bias indices (mean ± SEM) for the interpatch, patch, and LS regions in intact and callosotomized rats (see Results for statistical analysis). The number of rats analyzed in each group is indicated. (*F*) Effectiveness of the callosotomy procedure. The sections shown were taken 6.0 mm (back panel) and 4.2 mm (front panel) from bregma. White arrow shows transection of the corpus callosum. Black arrowheads indicate borders of V1. LGN = lateral geniculate nucleus, LP = lateral posterior nucleus. Scale bars = 1.0 mm.

Ten-m3 showed interdigitation of ipsilateral and contralateral eye domains in V1 (Merlin et al. 2012). These authors hypothesize that segregation of eye domains is likely linked to abnormalities associated with the dramatic expansion of the ipsilateral projection. It will be interesting to determine to what extent the mechanisms mediating the segregation of eye domains in these mutant mice compare with those giving rise to the eye-specific segregation we have shown in normal, Long Evans rats.

The LS resembles a cortical strip in ferret V1 that adjoins the 17/18 border and receives subcortical input only from the contralateral eye (Ruthazer et al. 1999; White et al. 1999). The temporal retina in the ferret projects to both hemispheres (Vitek et al. 1985; Morgan et al. 1987), and the crossed projection likely innervates this continuous contralateral eye domain, conveying a representation of central portions of the ipsilateral visual field (White et al. 1999). The temporal retina in the rat also projects bilaterally (Lund et al. 1974; Reese and Cowey 1987), and the contralateral projection is thought to innervate a lateral strip in V1 (Lewis and Olavarria 1995). Our results are consistent with this interpretation and suggest that the LS is the target of projections from the contralateral temporal retina. Thus, the LS could be considered as a single contralateral eye domain that is likely homologous to the continuous contralateral eye band observed in ferret V1.

Comparison With Studies in the Cat

In the cat, callosal connections correlate with contralateral ODCs within a narrow strip known as the 17/18 transition zone (TZ), and with ipsilateral ODCs in regions of V1 located immediately medial to the TZ (Olavarria 2001, 2002; Alekseenko et al. 2005). Olavarria (1996) proposed that callosal linkages between these cortical regions are stabilized during development by influences delivered by bilateral projections from temporal retina. This mechanism would not only induce the formation of callosal patches, but also be responsible for the correlation of callosal patches with either contralateral or ipsilateral ODCs in different regions of V1 (see Fig. 9*B* in Olavarria 2001).

Since the temporal retina also projects bilaterally in the rat (Lund et al. 1974; Reese and Cowey 1987) it is possible that a similar mechanism operates in this rodent. Figure 10 illustrates our view of the relationship between retinal projections, eye-specific domains and point-to-point callosal connectivity (Lewis and Olavarria 1995) in Long Evans rats. The temporal retina of the right eye (colored dark gray) projects both to ipsilateral eye domains in the right CS (dark gray circular areas) and to the LS in the left hemisphere (dark gray strip). These cortical regions map the same sector of the left hemifield (colored dark gray) and are interconnected via callosal regions that overlap the dark gray circular areas in the CS of the right hemisphere, and the dark gray LS in the left hemisphere. Thus, as in the cat (Olavarria 2001, 2002), callosal connections in the rat correlate preferentially with ipsilateral eye domains in the CS and with contralateral eye input in the LS. Note that callosal connections link retinotopically matching, but anatomically nonmatching, locations (Lewis and Olavarria 1995; Olavarria 1996, 2001; Bosking et al. 2000; Olavarria and Hiroi 2003).

Binocularity in V1 Does Not Depend on Callosal Input

Figure 10 also illustrates that input from the ipsilateral eye to the ipsilateral eye domains in CS, as well as input from the contralateral eye to the LS can potentially be routed through the

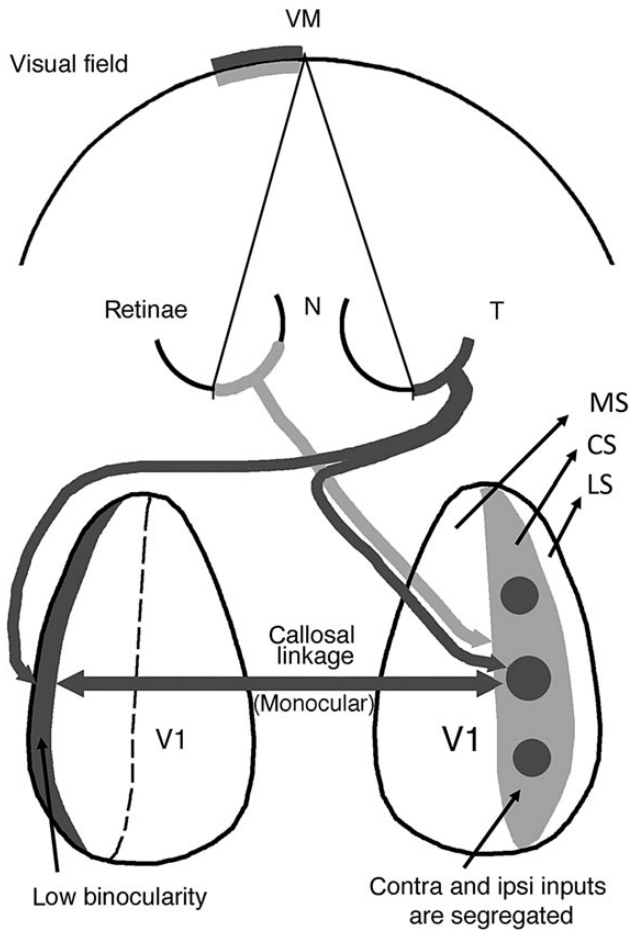

Figure 10. Diagram relating the patterns of retinal projections to eye-specific domains in V1 and to the callosal linkages established between these domains. For simplicity only projections from the right temporal (dark gray) and left nasal (light gray) retinas are shown and the geniculate relay stations have been omitted. This diagram summarizes our finding that callosal connections correlate preferentially with ipsilateral eye domains in the CS (dark gray circular areas in the right CS) and with contralateral eye input in the LS (dark gray strip at left). The pathway colored light gray illustrates that input from the left nasal retina to the right CS is distributed preferentially to noncallosally connected regions (light gray regions) surrounding the ipsilateral eye domains, being therefore unable to convey ipsilateral eye input transcallosally to the left LS. This diagram helps explain our observation that LS in hooded rats is strongly dominated by the contralateral eye. Dashed line indicates the medial border of the CS. T, temporal; N, nasal; MS, medial segment; CS, central segment; LS, lateral segment. Diagram is based on our present results as well as previous studies of the point-to-point callosal connectivity in rat visual cortex (Lewis and Olavarria 1995; Olavarria and Hiroi 2003).

callosal commissure. Consistent with this diagram, split optic chiasm experiments in the cat indicate that callosal connections convey contralateral eye input to the TZ (Berlucchi and Rizzolatti 1968; Lepore and Guillemot 1982; Rochefort et al. 2007). In addition, Cerri et al. (2010) showed that callosal connections convey ipsilateral eye input to the binocular region in rat V1. These authors recorded from V1 after injecting TTX into the ipsilateral thalamus to block crossed and uncrossed retinal projections and reported that the inactivation primarily reduced the responses driven by the contralateral eye.

However, in agreement with previous studies in hooded rats (Adams and Forrester 1968; Silveira et al. 1989; but see Restani et al. 2009) and cat (Minciacchi and Antonini 1984), we found that section of the callosum did not significantly alter the ocular dominance map in the CS and LS, indicating that

binocularity at sites within callosal territories does not depend significantly on callosal input. Although at first sight these results appear to contradict the previous studies mentioned in the paragraph above, they are consistent with the hypothesis that callosal fibers link cortical sites that are under the influence of the same temporal retina (see Fig. 10), as well as with the prediction that section of the callosal commissure would not have a significant effect on binocularity in V1 (Olavarria 2001, 2002). As illustrated in Figure 10, callosal input to either the LS or to ipsilateral eye domains largely duplicates the direct retino-thalamo-cortical input to these cortical regions originating from the same temporal retina. Thus, either the callosal connections or the retino-thalamo-cortical projection would be able to sustain visual cortical activity when the other pathway is abolished.

Why is the LS Largely Monocular?

Studies in albino rats (Diao et al. 1983) and sheep (Pettigrew et al. 1984) show that a region corresponding to the LS is highly binocular, and that input from the ipsilateral eye to this region comes through the callosum. In contrast, we found that the LS is strongly dominated by the contralateral eye in spite of the fact that the LS is richly innervated by the callosum. Why are callosal connections in hooded rats unable to relay indirect input from the ipsilateral eye to the LS? Figure 10 illustrates that the LS in the left hemisphere (dark gray strip) cannot receive transcallosal input from the retinotopically matched nasal retina in the ipsilateral eye (colored light gray) because the regions innervated by this eye in the contralateral, right CS (light gray areas) are largely acallosal. However, if both the light and dark gray territories were intermixed in the right CS, as it would occur in an animal without ocular dominance domains, then input from the left hemiretina (light gray) arriving to the right CS would have access to the left LS through the callosum, leading to an increased binocularity in the left LS. Thus, our findings in Long Evans rats raise the possibility that albino rats and sheep lack segregated ocular dominance domains in V1, a possibility that is consistent with our preliminary results in albino rats (Olavarria et al., unpublished data) and with previous findings in the sheep (Pettigrew et al. 1984). In this context, our observation that callosal connections do not relay significant input from the ipsilateral eye to the LS further supports our findings that eye-specific domains are functionally segregated in Long Evans rats.

In conclusion, we have shown that Long Evans rats have anatomically and functionally segregated eye-specific domains and patchy callosal connections. We also showed that patches of callosal connections correlate with specific sets of ocular dominance domains just as they do in the cat. These observations suggest that at least some aspects of the modular architecture of rat visual cortex develop according to principles observed in higher species. They also raise the possibility that modular architecture in visual cortex is more conserved among rodents, carnivores, and primates than previously thought. Our findings offer a new model for studying aspects of neural circuitry relevant to the emergence of modular architecture in visual cortex, as well as molecular and other factors involved in the development and plasticity of binocular vision.

Supplementary Material

Supplementary material can be found at: http://www.cercor.oxfordjournals.org/

Funding

This work was supported by a Royalty Research Fund award, University of Washington to J.F.O., and by National Institutes of Health grant R01NSO70022. R.J.L. was supported by National Institute of Health Vision Training Grant T32 EY7031. T.T. was supported by a postdoctoral fellowship for research abroad from the Japan Society for the Promotion of Science.

Notes

We thank H. Sherk for her comments and technical advice, H. Lu and A. Andelin for helping with experiments, R. Hiroi for participating in initial experiments, and L.E. Trice and M.R. Feurtado, Vanderbilt University, for technical assistance. *Conflict of Interest*: None declared.

References

Adams AD, Forrester JM. 1968. The projection of the rat's visual field on the cerebral cortex. Q J Exp Physiol Cogn Med Sci. 53:327–336.

Alekseenko SV, Toporova SN, Makarov FN. 2005. Neuronal connection of the cortex and reconstruction of the visual space. Neurosci Behav Physiol. 35:435–442.

Anderson PA, Olavarria J, Van Sluyters RC. 1988. The overall pattern of ocular dominance bands in cat visual cortex. J Neurosci. 8:2183–2200.

Antonini A, Fagiolini M, Stryker MP. 1999. Anatomical correlates of functional plasticity in mouse visual cortex. J Neurosci. 19: 4388–4406.

Berlucchi G, Rizzolatti G. 1968. Binocularly driven neurons in visual cortex of split-chiasm cats. Science. 159:308–310.

Bosking WH, Kretz R, Pucak ML, Fitzpatrick D. 2000. Functional specificity of callosal connections in tree shrew striate cortex. J Neurosci. 20:2346–2359.

Caleo M, Lodovichi C, Pizzorusso T, Maffei L. 1999. Expression of the transcription factor Zif268 in the visual cortex of monocularly deprived rats: effects of nerve growth factor. Neuroscience. 91:1017–1026.

Caviness VS. 1975. Architectonic map of neocortex of the normal mouse. J Comp Neurol. 164:247–263.

Cerri C, Restani L, Caleo M. 2010. Callosal contribution to ocular dominance in rat primary visual cortex. Eur J Neurosci. 32:1163–1169.

Chaudhuri A, Matsubara JA, Cynader MS. 1995. Neuronal activity in primate visual cortex assessed by immunostaining for the transcription factor Zif268. Vis Neurosci. 12:35–50.

Chaudhuri A, Nissanov J, Larocque S, Rioux L. 1997. Dual activity maps in primate visual cortex produced by different temporal patterns of Zif268 mRNA and protein expression. Proc Natl Acad Sci USA. 94:2671–2675.

Cusick DG, Lund RD. 1981. The distribution of the callosal projections to the occipital visual cortex in rats and mice. Brain Res. 214:239–259.

Diao YC, Wang YK, Pu ML. 1983. Binocular responses of cortical cells and the callosal projection in the albino rat. Exp Brain Res. 49: 410–418.

Dräger UC. 1974. Autoradiography of tritiated proline and fucose transported transneuronally from the eye to the visual cortex in pigmented and albino mice. Brain Res. 82:284–292.

Dräger UC. 1975. Receptive fields of single cells and topography in mouse visual cortex. J Comp Neurol. 160:269–290.

Fagiolini M, Pizzorusso T, Berardi N, Domeneci L, Maffei L. 1994. Functional postnatal development of the rat primary visual cortex and the role of visual experience: dark rearing and monocular deprivation. Vis Res. 34:709–720.

Gallyas F. 1979. Silver staining of myelin by means of physical development. Neurol Res. 1:203–209.

Gerfen CR, O'Leary DD, Cowan WM. 1982. A note on the transneuronal transport of wheat germ agglutinin-conjugated horseradish peroxidase in the avian and rodent visual systems. Exp Brain Res. 48:443–448.

Girman SV, Sauve Y, Lund RD. 1999. Receptive field properties of single neurons in rat primary visual cortex. J Neurophysiol. 82:301–311.
Gordon JA, Stryker MP. 1996. Experience-dependent plasticity of binocular responses in the primary visual cortex of the mouse. J Neurosci. 16:3274–3286.
Hata Y, Stryker MP. 1994. Control of thalamocortical afferent rearrangement by postsynaptic activity in developing visual cortex. Science. 265:1732–1735.
Hirokawa J, Watakabe A, Ohsawa S, Yamamori T. 2008. Analysis of area-specific expression patterns of RORbeta, ER81 and Nurr1 mRNAs in rat neocortex by double in situ hybridization and cortical box method. PLoS One. 3:e3266.
Horton JC, Adams DL. 2005. The cortical column: a structure without a function. Phil Trans R Soc B. 360:837–862.
Horton JC, Hocking DR. 1996. Anatomical demonstration of ocular dominance columns in striate cortex of the squirrel monkey. J Neurosci. 16:5510–5522.
Horton JC, Hocking DR, Adams DL. 2000. Rapid identification of ocular dominance columns in macaques using cytochrome oxidase, Zif268, and dark-field microscopy. Vis Neurosci. 17:495–508.
Hubel DH, Wiesel TN. 1962. Receptive fields, binocular interaction and functional architecture in the cat's visual cortex. J Comp Physiol. 160:106–154.
Ichinohe N, Fujiyama F, Kaneko T, Rockland KS. 2003. Honeycomb-like mosaic at the border of layers 1 and 2 in the cerebral cortex. J Neurosci. 23:1372–1382.
Itaya SK. 1988. Transneuronal transport of WGA-HRP in immature rat visual pathways. Brain Res. 466:83–88.
Itaya SK, Van Hoesen GW. 1982. WGA-HRP as a transneuronal marker in the visual pathways of monkey and rat. Brain Res. 236:199–204.
Kageyama GH, Gallivan ME, Gallardo KA, Robertson RT. 1990. Relationships between patterns of acetylcholinesterase activity and geniculocortical terminal fields in developing and mature rat visual cortex. Dev Brain Res. 53:139–144.
Kalatsky VA, Stryker MP. 2003. New paradigm for optical imaging: temporally encoded maps of intrinsic signal. Neuron. 38:529–545.
Katz LC, Burkhalter A, Dreyer WJ. 1984. Fluorescent latex microspheres as a retrograde neuronal marker for *in vivo* and *in vitro* studies of visual cortex. Nature. 310:498–500.
Krieg WJS. 1946. Connections of the cerebral cortex I. The albino rat. A. Topography of the cortical areas. J Comp Neurol. 84:221–275.
Laing RJ, Bock AS, Lasiene J, Olavarria JF. 2012. Role of retinal input on the development of striate–extrastriate patterns of connections in the rat. J Comp Neurol. 520:3256–3276.
Lepore F, Guillemot JP. 1982. Visual receptive field properties of cells innervated through the corpus callosum in the cat. Exp Brain Res. 46:413–424.
LeVay S, Gilbert CD. 1976. Laminar pattern of geniculocortical projection in the cat. Brain Res. 113:1–19.
Lewis JW, Olavarria JF. 1995. Two rules for callosal connectivity in striate cortex of the rat. J Comp Neurol. 361:119–137.
Lund RD, Lund JS, Wise RP. 1974. The organization of the retinal projection to the dorsal lateral geniculate nucleus in pigmented and albino rats. J Comp Neurol. 158:383–404.
Markstahler U, Bach M, Spatz WB. 1998. Transient molecular visualization of ocular dominance columns (ODCs) in normal adult marmosets despite the desegregated termination of the retino-geniculocortical pathways. J Comp Neurol. 393:118–134.
Merlin S, Horng S, Marotte LR, Sur M, Sawatari A, Leamey CA. 2012. Deletion of Ten-m3 induces the formation of eye dominance domains in mouse visual cortex. Cereb Cortex. 23:763–774.
Mesulam MM. 1978. Tetramethyl benzidine for horseradish peroxidase neurohistochemistry: a non-carcinogenic blue reaction product with superior sensitivity for visualizing neural afferents and efferents. J Histochem Cytochem. 26:106–117.
Metín C, Godement P, Imbert M. 1988. The primary visual cortex in the mouse: receptive field properties and functional organization. Exp Brain Res. 69:594–612.
Minciacchi D, Antonini A. 1984. Binocularity in the visual cortex of the adult cat does not depend on the integrity of the corpus callosum. Behav Brain Res. 13:183–192.
Morgan JE, Henderson Z, Thompson ID. 1987. Retinal decussation patterns in pigmented and albino ferrets. Neurosci. 20:519–535.
Mrsic-Flögel TD, Hofer SB, Ohki K, Reid RC, Bonhöffer T, Hübener M. 2007. Homeostatic regulation of eye-specific responses in visual cortex during ocular dominance plasticity. Neuron. 54:961–972.
Ohki K, Chung S, Ch'ng YH, Kara P, Reid RC. 2005. Functional imaging with cellular resolution reveals precise micro-architecture in visual cortex. Nature. 433:597–603.
Ohki K, Reid RC. 2007. Specificity and randomness in the visual cortex. Curr Opin Neurobiol. 17:401–407.
Olavarria J, Van Sluyters RC. 1984. Callosal connections of the posterior neocortex in normal-eyed, congenitally anophthalmic, and neonatally enucleated mice. J Comp Neurol. 230:249–268.
Olavarria J, Van Sluyters RC. 1985. Organization and postnatal development of callosal connections in the visual cortex of the rat. J Comp Neurol. 239:1–26.
Olavarria JF. 2001. Callosal connections correlate preferentially with ipsilateral domains in cat areas 17 and 18, and with contralateral domains in the 17/18 transition zone. J Comp Neurol. 433:441–457.
Olavarria JF. 2002. Influence of topography and ocular dominance on the functional organization of callosal connections in cat striate cortex. In: Payne B, Peters A, editors. The cat primary visual cortex. New York (NY): Academic Press. p. 259–294.
Olavarria JF. 1996. Non-mirror-symmetric patterns of callosal linkages in areas 17 and 18 in cat visual cortex. J Comp Neurol. 366: 643–655.
Olavarria JF, Hiroi R. 2003. Retinal influences specify cortico-cortical maps by postnatal day six in rats and mice. J Comp Neurol. 459:156–172.
Pettigrew JD, Ramachandran VS, Bravo H. 1984. Some neural connections subserving binocular vision in ungulates. Brain Behav Evol. 24:65–93.
Reese BE, Cowey A. 1987. The crossed projection from the temporal retina to the dorsal lateral geniculate nucleus in the rat. Neurosci. 20:951–959.
Reiner A, Veenman CL, Medina L, Jiao Y, Del Mar N, Honig MG. 2000. Pathway tracing using biotinylated dextran amines. J Neurosci Meth. 103:23–37.
Restani L, Cerri C, Pietrasanta M, Gianfranceschi L, Maffei L, Caleo M. 2009. Functional masking of deprived eye responses by callosal input during ocular dominance plasticity. Neuron. 64: 707–718.
Richter CP, Warner CL. 1974. Comparison of Weigert stained sections with unfixed, unstained sections for study of myelin sheaths. Proc Natl Acad Sci USA. 71:598–601.
Rochefort NL, Buzas P, Kisvarday ZF, Eysel UT, Milleret C. 2007. Layout of transcallosal activity in cat visual cortex revealed by optical imaging. Neuroimage. 36:804–821.
Ruthazer ES, Basker GE, Stryker MP. 1999. Development and organization of ocular dominance bands in primary visual cortex of the sable ferret. J Comp Neurol. 407:151–165.
Schlingensiepen KH, Lüno K, Brysch W. 1991. High basal expression of the zif/268 immediate early gene in cortical layers IV and VI, in CA1 and in the corpus striatum—an in situ hybridization study. Neurosci Lett. 122:67–70.
Shatz CJ, Lindstrom S, Wiesel TN. 1977. The distribution of afferents representing the right and left eyes in the cat's visual cortex. Brain Res. 131:103–116.
Sheng M, Greenberg ME. 1990. The regulation and function of c-Fos and other immediate early genes in the nervous system. Neuron. 4:477–485.
Silveira LC, Heywood CA, Cowey A. 1989. Direct and transcallosal contribution to the cortical visual evoked response in rats. Behav Brain Res. 31:291–294.
Takahata T, Higo N, Kaas JH, Yamamori T. 2009. Expression of immediate-early genes reveals functional compartments within ocular dominance columns after brief monocular inactivation. Proc Natl Acad Sci USA. 106:12151–12155.

Takahata T, Miyashita M, Tanaka S, Kaas JH. 2014. Identification of ocular dominance domains in New World owl monkeys by immediate-early gene expression. Proc Natl Acad Sci USA. 111: 4297–4202.

Thurlow GA, Cooper RM. 1988. Metabolic activity in striate and extrastriate cortex in the hooded rat: contralateral and ipsilateral eye input. J Comp Neurol. 274:595–607.

Tootell RB, Hamilton SL, Silverman MS, Switkes E. 1988. Functional anatomy of macaque striate cortex. I. Ocular dominance, binocular interactions, and baseline conditions. J Neurosci. 8:1500–1530.

Trojanowski JQ, Gonatas J, Gonatas NK. 1981. A light and electron microscopic study of the intraneural transport of horseradish peroxidase and wheat germ agglutinin-peroxidase conjugates in the rat visual system. J Neurocytol. 10:441–456.

van Brussel L, Gerits A, Arckens L. 2009. Identification and localization of functional subdivisions in the visual cortex of the adult mouse. J Comp Neurol. 514:107–116.

Van Hooser SD. 2007. Similarity and diversity in visual cortex: is there a unifying theory of cortical computation? Neuroscientist. 13:639–656.

Van Hooser SD, Heimel JA, Chung S, Nelson SB. 2006. Lack of patchy horizontal connectivity in primary visual cortex of a mammal without orientation maps. J Neurosci. 26:7680–7692.

Van Hooser SD, Heimel JA, Chung S, Nelson SB, Toth LJ. 2005. Orientation selectivity without orientation maps in visual cortex of a highly visual mammal. J Neurosci. 25:19–28.

Vitek DJ, Schall JD, Leventhal AG. 1985. Morphology, central projections, and dendritic field orientation of retinal ganglion cells in the ferret. J Comp Neurol. 241:1–11.

White LE, Bosking WH, Williams SM, Fitzpatrick D. 1999. Maps of central visual space in ferret V1 and V2 lack matching inputs from the two eyes. J Neurosci. 19:7089–7099.

Zilles K, Zilles B, Schleicher A. 1980. A quantitative approach to cytiarchitectonics. Anat Embryol. 159:335–360.